The Astrophysical Journal, 720:1318–1324, 2010 September 10 doi:10.1088/0004-637X/720/2/1318

THE INFLUENCE OF THE MASS RATIO ON THE ACCELERATION OF PARTICLES BY FILAMENTATION INSTABILITIES

Thomas Burkart, Oliver Elbracht, Urs Ganse, and Felix Spanier
Lehrstuhl für Astronomie, Universität Würzburg, Am Hubland, D-97074 Würzburg, Germany; fspanier@astro.uni-wuerzburg.de
Received 2009 August 20; accepted 2010 July 11; published 2010 August 19

ABSTRACT

Almost all sources of high-energy particles and photons are associated with jet phenomena. Prominent sources of such highly relativistic outflows are pulsar winds, active galactic nuclei (AGNs), and gamma-ray bursts. The current understanding of these jets assumes diluted plasmas which are best described as kinetic phenomena. In this kinetic description, particle acceleration to ultrarelativistic speeds can occur in completely unmagnetized and neutral plasmas through insetting effects of instabilities. Even though the morphology and nature of particle spectra are understood to a certain extent, the composition of the jets is not known yet. While Poynting-flux-dominated jets (e.g., occurring in pulsar winds) are certainly composed of electron–positron plasmas, the understanding of the governing physics in AGN jets is mostly unclear. In this paper, we investigate how the constituting elements of an electron–positron–proton plasma behave differently under the variation of the fundamental mass ratio m_p/m_e. We initially studied unmagnetized counterstreaming plasmas using fully relativistic three-dimensional particle-in-cell simulations to investigate the influence of the mass ratio on particle acceleration and magnetic field generation in electron–positron–proton plasmas. We covered a range of mass ratios m_p/m_e between 1 and 100 with a particle number composition of n_{p^+}/n_{e^+} of 1 in one stream, therefore called the pair-proton stream. Protons are injected in the other one, therefore from now on called the proton stream, whereas electrons are present in both to guarantee charge neutrality in the simulation box. We find that with increasing proton mass the instability takes longer to develop and for mass ratios >20 the particles seem to be accelerated in two phases which can be accounted for by the individual instabilities of the different species. This means that for high mass ratios the coupling between electrons/positrons and the heavier protons, which occurs in low mass ratios, disappears.

Key words: acceleration of particles – galaxies: jets – instabilities – methods: numerical – plasmas

Online-only material: color figures

1. INTRODUCTION

Radiation observed from astrophysical systems such as gamma-ray bursts or active galactic nuclei usually possesses a nonthermal emission spectrum. This is believed to arise from particle acceleration in the vicinity of relativistic shocks or within the counterstreaming plasma itself.

In recent particle-in-cell (PiC) simulations it has been shown that most particle acceleration occurs within the jet (Nishikawa et al. 2003, 2005, 2006, 2008, 2010; Chang et al. 2008; Spitkovsky 2008a; Dieckmann et al. 2008; Frederiksen et al. 2004; Hededal et al. 2004; Hededal & Nishikawa 2005; Martins et al. 2009; Ramirez-Ruiz et al. 2007; Silva et al. 2003) and is mostly caused by plasma instabilities such as the Weibel (Weibel 1959) or two-stream instability (Buneman 1958). Both instabilities create current filaments with surrounding magnetic fields and are therefore a plausible source for particle acceleration and the generation of observed long-lasting magnetic fields. Particle acceleration can also occur along with shocks where first-order Fermi acceleration (Fermi 1949) is assumed to be the relevant process, which was shown by kinetic simulations only recently (Spitkovsky 2008b).

In the present work, we focus on the main properties of the plasma instabilities and describe the influence of the fundamental mass ratio m_p/m_e in mixed electron–positron–proton compositions by means of relativistic three-dimensional simulations of counterstreaming plasmas.

The paper is organized as follows. In Section 2, the underlying code is described briefly. In Section 3, we illustrate the setup of the performed simulations. In Section 4, we present the results of our simulations which we discuss and draw some conclusion in Section 5.

2. DESCRIPTION OF THE CODE

PiC simulations are an essential tool in understanding relativistic collisionless plasma physics. Therefore, we developed a three-dimensional fully relativistic MPI-parallelized PiC code called ACRONYM (Another Code for moving Relativistic Objects, Now with Yee lattice and Macroparticles). Maxwell's equations are evolved in time by employing a second-order leapfrog scheme (see, e.g., Taflove & Hagness 2005). The particles affect the electromagnetic fields through charge currents which are deposited on the grid by using a second-order triangular-shaped cloud scheme (see, e.g., Hockney & Eastwood 1988) adopted from Esirkepov (2001). The particles are moved via a second-order force interpolation within the Boris push (Boris 1970). In order to guarantee that the divergence of the magnetic field remains close to zero, the electric and magnetic fields are stored in the form of a staggered grid, the so-called Yee lattice (Yee 1966). With this setup the code is second order both in space and time.

Extensive tests of the code have been successfully completed from which we conclude that the total relative error in energy conservation is less than 3×10^{-5} and the divergence of the magnetic field stays below a value $|\nabla \vec{B}/B| < 10^{-12}/\lambda_D$ in the simulated space for all times.

Table 1
Setup of the Simulations Performed

m_p/m_e	$\Delta t\ (\omega_p^{-1})$	Δx (cm)	Number of Cells	Number of Ion Skin Depths
1.0	0.0498	23225	128 × 128 × 512	120 × 120 × 480
5.0	0.0385	23107	128 × 128 × 512	57 × 57 × 228
20.0	0.0360	21614	128 × 128 × 512	28 × 28 × 112
42.8	0.0355	21338	128 × 128 × 512	20 × 20 × 80
100.0	0.0408	21198	128 × 128 × 512	13 × 13 × 52
100.0	0.0574	29830	256 × 256 × 512	36 × 36 × 72

3. SIMULATION SETUP

In the simulations presented here we use two counterstreaming plasma populations, one representing the background medium consisting of $6e^-$ and $6p^+$ per cell (proton stream) and the other incorporating the jet containing $4e^-$, $2e^+$, and $2p^+$ per cell (pair-proton stream), from which we find the background density ratio $n_{\rm jet}/n_{\rm bg} = 2/3$ and the ratio $n_{p^+}/n_{e^+} = 1$ in the pair-proton stream. In the lab frame (the rest frame of the simulation box), the two streams are counterstreaming along the z-direction with a Lorentz factor $\gamma = 10\,(\beta = v/c = 0.995)$ each, the electron distribution has a thermal velocity of $v_{{\rm th},e} = 0.1c$ in every direction in the rest frame of the moving medium, and the thermal velocity of the protons is $v_{{\rm th},p} = 0.1c \cdot (m_p/m_e)^{-1}$. This setup resembles situations as they are believed to exist in jets running into the interstellar or intergalactic medium.

Three-dimensional simulations with five different compositions of counterstreaming plasmas using 128 × 128 × 512 cells with a total of 167 million particles (20 particles per cell) and mass ratios m_p/m_e between 1 and 100 have been performed. In addition to that another simulation with a mass ratio of 100 with twice the number of cells in each of the perpendicular directions (and therefore four times more particles) has been performed in order to show the influence of the periodic boundary conditions. As pointed out by Fonseca et al. (2008), 20 particles per unit cell (on average) in combination with quadratic particle interpolation are sufficient to eliminate most of the numerical noise. Nevertheless, we have performed simulations up to twice the numbers of particles per cell and no significant changes were observed.

Periodic boundary conditions have been applied in all three dimensions. Due to the quick development of the self-consistent electromagnetic fields it is redundant to solve Poisson's equation at the initial time and the fields can be initialized with zero without loss of generality.

The cell size is set to be equal to the Debye length of the plasma, $\Delta x = \lambda_D = (k_{\rm B}T/4\pi n_e e^2)^{1/2}$, and the time step is restricted by the CFL criterion, $c \cdot \Delta t < \Delta x/\sqrt{3}$. This results in a Δt between $0.035\omega_p^{-1}$ and $0.050\omega_p^{-1}$ (normalized to the plasma frequency $\omega_p = (4\pi e^2 n/m_e)^{1/2}$) and the cell size Δx ranges from 2×10^4 cm to 3×10^4 cm depending on the different mass ratios employed. The simulations were evolved for 2500–4500 time steps to roughly 120–220 ω_p^{-1} (the exact numbers for each simulation can be found in Table 1). The characteristic scales of interest in a counterstreaming electron–positron–proton plasma are of the order of several proton skin depths, $c/\omega_{pi} = (\gamma m_p c^2/4\pi e^2 n)^{1/2}$, for a plasma with the density n and the average proton energy $\gamma m_p c^2$.

4. SIMULATION RESULTS

The results of our simulations can be divided into two main findings: (1) new insights into the evolutionary behavior of two-stream instabilities in multi-component plasma and (2) the change in the distribution function of the particles, in particular the acceleration caused by the instability.

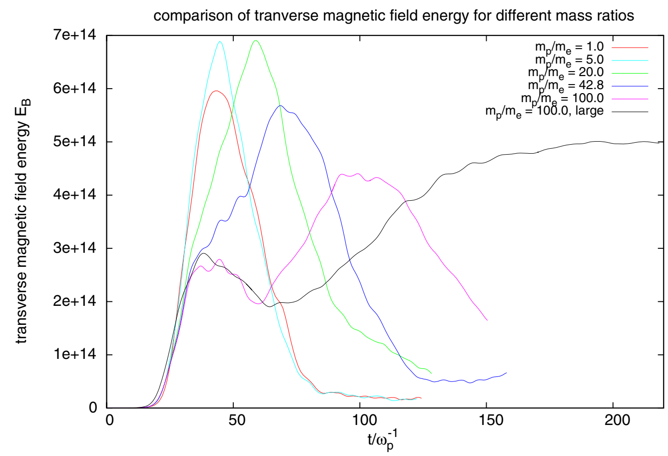

Figure 1. Comparison of the time evolution of the transverse magnetic field energy for different mass ratios. With increasing mass ratio the instability takes longer to develop. For the two highest mass ratios one notices that the instability develops in two phases.

(A color version of this figure is available in the online journal.)

Due to the huge amount of data, simulation results have been written every tenth step for the fields (electric and magnetic fields, currents) and every hundredth step for particle data.

4.1. Analysis of the Fields and Currents

In this section, we analyze the evolutionary behavior of the electric and magnetic fields and the currents in the simulations conducted. From previous simulations of filamentation instabilities in pair plasmas (see, e.g., Silva et al. 2003) it is well known how magnetic and electric fields evolve. We compare the behavior of plasmas with different mass ratios. The most significant quantity in this context is the transverse magnetic field energy averaged over the entire computational domain $B_\perp^2 = (B_x^2 + B_y^2)$, since strong magnetic fields are essential to create and maintain the flux tubes observed in kinetic instabilities, furthermore the point in time the instability peak occurs and also the existence of a second peak, respectively.

In Figure 1, we therefore compare the time evolution of the transverse magnetic field energy $B_\perp$ computed in the lab frame as a function of different mass ratios m_p/m_e.

It is evident that the maximum value of the transverse magnetic field energy reached in the different simulations is comparable, even though it has to be noted that for the non-pair plasma the maximum energy can only be found in the second peak. The development of the second peak shows a nicely observable dependence on the fundamental mass ratio: for the lower mass ratios no two peak structure can be seen, while with increasing mass ratio a clear distinction can be made.

When looking at the time until the instability fully develops, one can see that for higher mass ratios m_p/m_e it takes longer to reach the peak value for the magnetic field. If one compares simulations with mass ratios of 1 and 100 one can explain what is happening in the counterstreaming plasma: first an electron–positron instability develops almost simultaneously for both mass ratios (single peak for mass ratio 1 and first peak for mass ratio 100). If a third and heavier species exists another peak will be apparent at later times (which can be seen in Figure 1). This behavior is not observable for medium

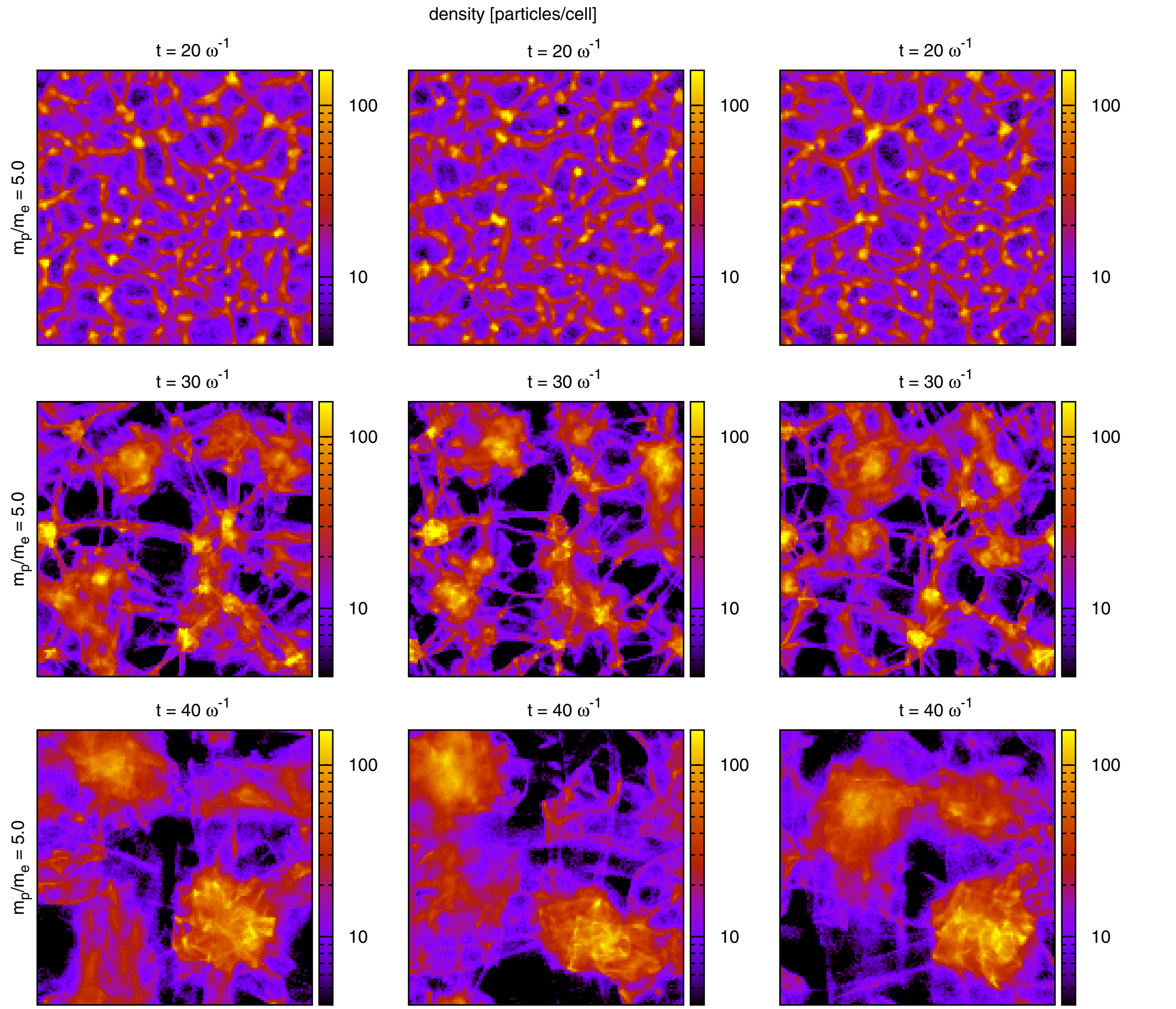

Figure 2. Development and merging of the flux tubes for the simulation with $m_p/m_e = 5.0$ and a resolution of $128 \times 128 \times 512$ cells. The colors pertain to the particle density (in particles per cell) shown at three different locations along the direction of streaming (at 100, 300, and 500 Δx). One can see the flux tubes developing and merging over time. Both flux tubes have about the same strength, which shows that the instabilities of the electrons/positrons and the protons are still strongly coupled for this mass ratio.

(A color version of this figure is available in the online journal.)

mass ratio simulations since both peaks overlap and cannot be distinguished anymore.

The existence of two instabilities in the plasma has important impact on the amplitude and duration of the instability: clearly the instability lasts longer for the high mass ratio simulations, since in this case the heavy protons are accelerated slower compared to the lighter electrons/positrons but are able to stabilize the flux tubes for a longer period of time. Another result to note is that the maximum amplitude decreases with increasing mass ratio. This effect can be attributed to the lower number of particles constituting each instability.

To inspect the effect of employed mass ratios on the temporal evolution of instabilities, we looked at the nature of the flux tubes more closely. The flux tubes in the simulations with mass ratios of $m_p/m_e = 5.0$ and $m_p/m_e = 100.0$ are illustrated in Figures 2 and 3, respectively, which show the particle number density in particles per cell at three different locations perpendicular to the direction of streaming. The pictures in Figure 2 are chosen such that the uppermost row shows the onset of the instability and the lowest pictures are roughly taken at the time the maximum of the instability occurs (cf. Figure 1). In Figure 3, the upper row of slices is taken at the moment the electron/positron instability peaks, the second set of pictures shows the time between the two instabilities (compare with the black curve in Figure 1 at $80\omega_p^{-1}$), and the last set shows the point in time when the proton instability reaches its peak. Both simulations show the archetypical behavior of filamentation instabilities: flux tubes develop, which in turn merge until only two flux tubes survive. But for the high mass ratio simulations this whole process happens twice. In an early stage (which resembles the first peak

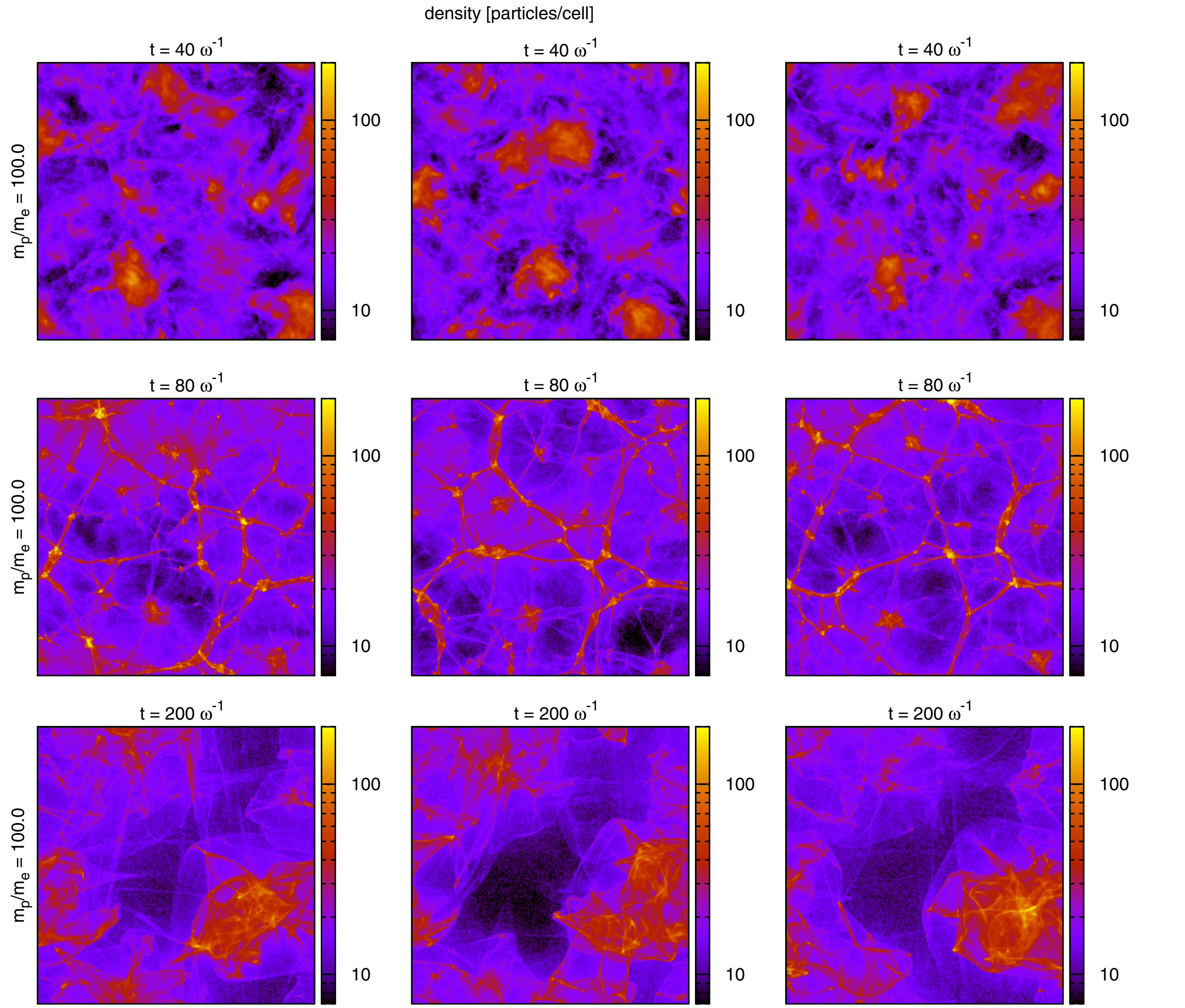

Figure 3. Development and merging of the flux tubes for the simulation with $m_p/m_e = 100.0$ and a resolution of $256 \times 256 \times 512$ cells. The colors pertain to the particle density (in particles per cell) shown at three different locations along the direction of streaming (at 100, 300, and 500 Δx). In the upper three pictures it is seen that first the flux tubes develop, later they nearly vanish (which corresponds to the dip in the magnetic field energy in Figure 1 in the black curve at $80\omega_p^{-1}$), and then the flux tube in the lower right corner grows stronger (lower set of pictures). This can be attributed to the independent instabilities at high mass ratios.

(A color version of this figure is available in the online journal.)

of the instability in Figure 1) flux tubes arise. In a later stage (second peak) flux tubes of different strengths exist, one of them is more pronounced. The explanation is that during the first stage of the instability the flux tubes are carrying more of the lighter particles. The second stage is then associated with a flux tube of heavier particles which takes longer to develop, but is also able to exist for a much longer time span.

The combination of Figures 1–3 suggests that the instability is evolving in two phases. In the first phase light particles are accelerated and in the second phase the heavier particles are also involved in the instability. For mass ratios of $m_p/m_e \lesssim 20.0$ the instabilities and therefore particle acceleration of the two species cannot be separated. There are two possible reasons for this: either the coupling of the two species is still strong enough to co-accelerate the heavier particles or the time scales of the two instabilities are still matching rather well. A strong argument for the second option is the fact that the instability time scale for the heavy species increases less than linear with the mass ratio for a certain size of the computational domain.

Considering only mass ratios $m_p/m_e > 20.0$, the instabilities are clearly separated which is also apparent in the double-hump structure in the energy diagrams of Figures 1 and 3 illustrating the development of the flux tubes in two phases.

In the larger simulation (twice the size in the perpendicular directions) it takes even longer for the proton instability to develop because the flux tubes have more space to develop and therefore it takes longer for them to merge until only two are left. This is also the reason for the slightly different slopes in the two simulations with mass ratio 100. The maxima and minima of the magnetic energy occur around the point in time when the current density in the direction of streaming averaged over the whole computational domain changes its sign. When

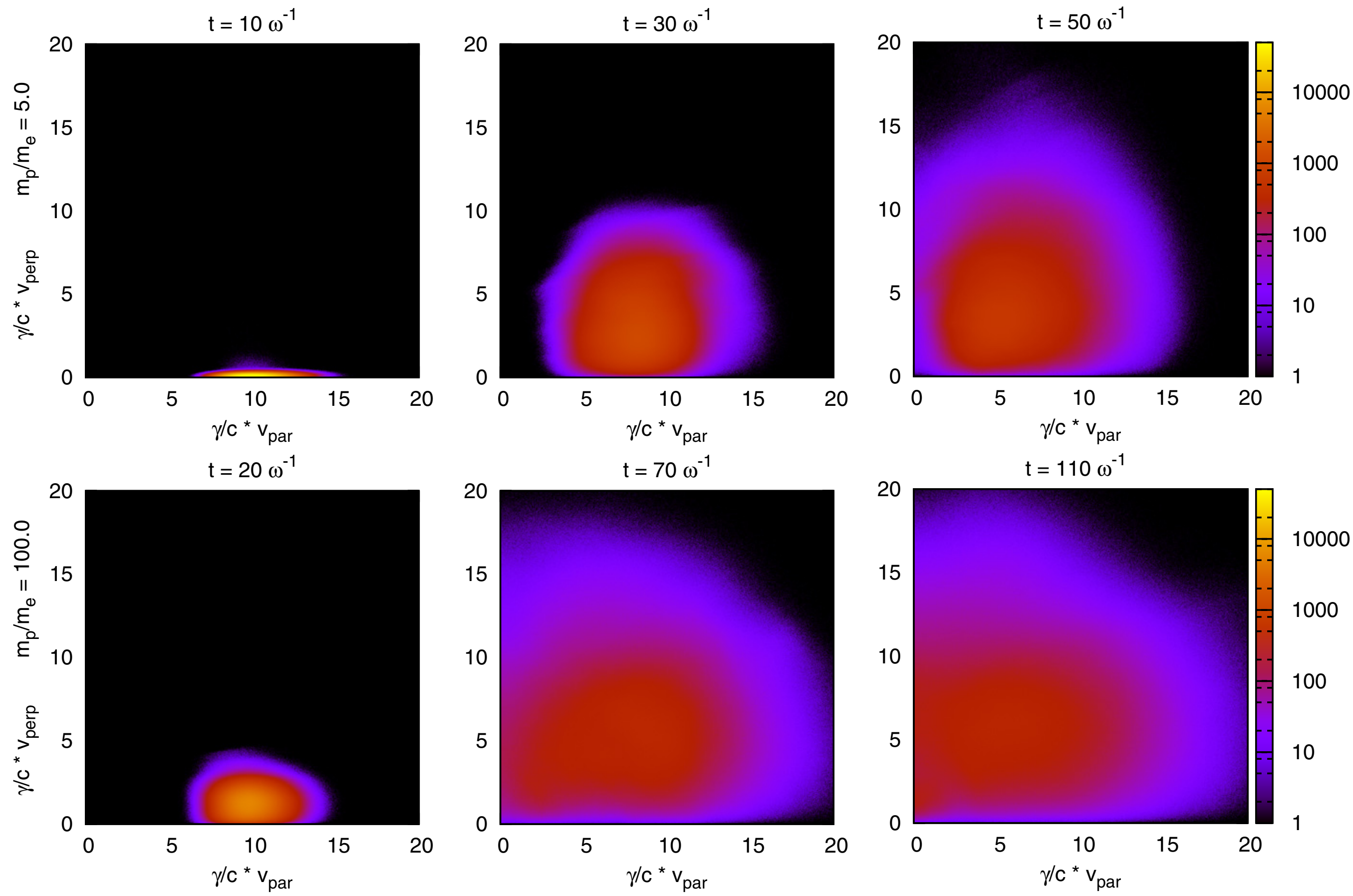

Figure 4. Development of the absolute value of the momentum distributions ($v_\perp/c \cdot \gamma$ over $v_{||}/c \cdot \gamma$) of all the electrons and positrons parallel and perpendicular to the direction of the original flow in the lab rest frame. First, one can state that most of the particle acceleration happens in the transverse direction. Second, for a mass ratio of $m_p/m_e = 5.0$ electrons and positrons are accelerated until the simulation stops, while for the higher mass ratio ($m_p/m_e = 100.0$) the electrons stop gaining energy around about $t = 70\omega^{-1}$.

(A color version of this figure is available in the online journal.)

(in the larger simulation) the proton instability kicks in (at around 65 ω_p^{-1}) the flux tubes are not yet fully merged down to two and therefore the proton instability does not grow with the same rate as in the smaller simulation. The resulting flux tubes around the maximum of the second instability still resemble the two flux tube regime as seen in the smaller simulations.

4.2. Particle Distribution

As described in Section 3 all simulations were initialized with thermal particle distributions (width of the thermal distribution $0.1c$ and $0.1c \cdot (m_p/m_e)^{-1}$ for electrons and protons, respectively) which are then boosted with a Lorentz factor of $\gamma = 10$ in either direction. While some particles gain a lot of energy during the simulation in total, the shape of the particle distribution is also changing. To analyze and quantify the change of the particle energy distributions we utilize two distinct types of graphs: (1) a two-dimensional plot in the lab frame relating the absolute value of the momentum parallel ($v_{||}/c \cdot \gamma$ with $v_{||} = |v_z|$) and perpendicular ($v_\perp/c \cdot \gamma$ with $v_\perp = (v_x^2 + v_y^2)^{\frac{1}{2}}$) to the initial streaming direction, respectively, and (2) a one-dimensional plot of the distribution of the particles speed in the lab frame.

In Figure 4, we show the time evolution of the electron and positron distribution (all electrons and positrons in both streams are plotted in a two-dimensional histogram for the mass ratios 5 (upper panels) and 100 (lower panels)). The same conjuncture is illustrated in Figure 5 for the protons, but the axes are different.

As expected, the particle distribution in the early stage of the simulation (before the onset of the first instability hump) is centered at the initial Lorentz boost $\gamma = 10$ with a thermal width of $0.1c$ for the electrons/positrons and $0.1c \cdot (m_p/m_e)^{-1}$ for the protons. Several electrons have already been accelerated and are streaming toward higher transverse velocities. At later times in the low mass ratio simulation one can see that both electrons and protons are getting accelerated simultaneously, as illustrated in the next two images in the upper rows of Figures 4 and 5. As emphasized before there is no clear distinction between low- and high-mass instabilities in this case, thus the simultaneous acceleration is clearly in agreement with the energy evolution (see Figure 1).

When going to higher mass ratios and early times (lower leftmost image of both figures) only the electrons are visible, as the protons still remain at their initial momentum. When the initial phase of the instability is over ($t \approx 70\omega_p^{-1}$) the electrons are no longer significantly accelerated. The protons are still gaining more energy until about $t = 110\omega_p^{-1}$, which is roughly at the maximum of the proton instability (see Figure 1 for comparison). This supports the idea of two almost separated instabilities.

In both cases, the particle distributions show a diffusion-like behavior: the initial distribution in the parallel direction

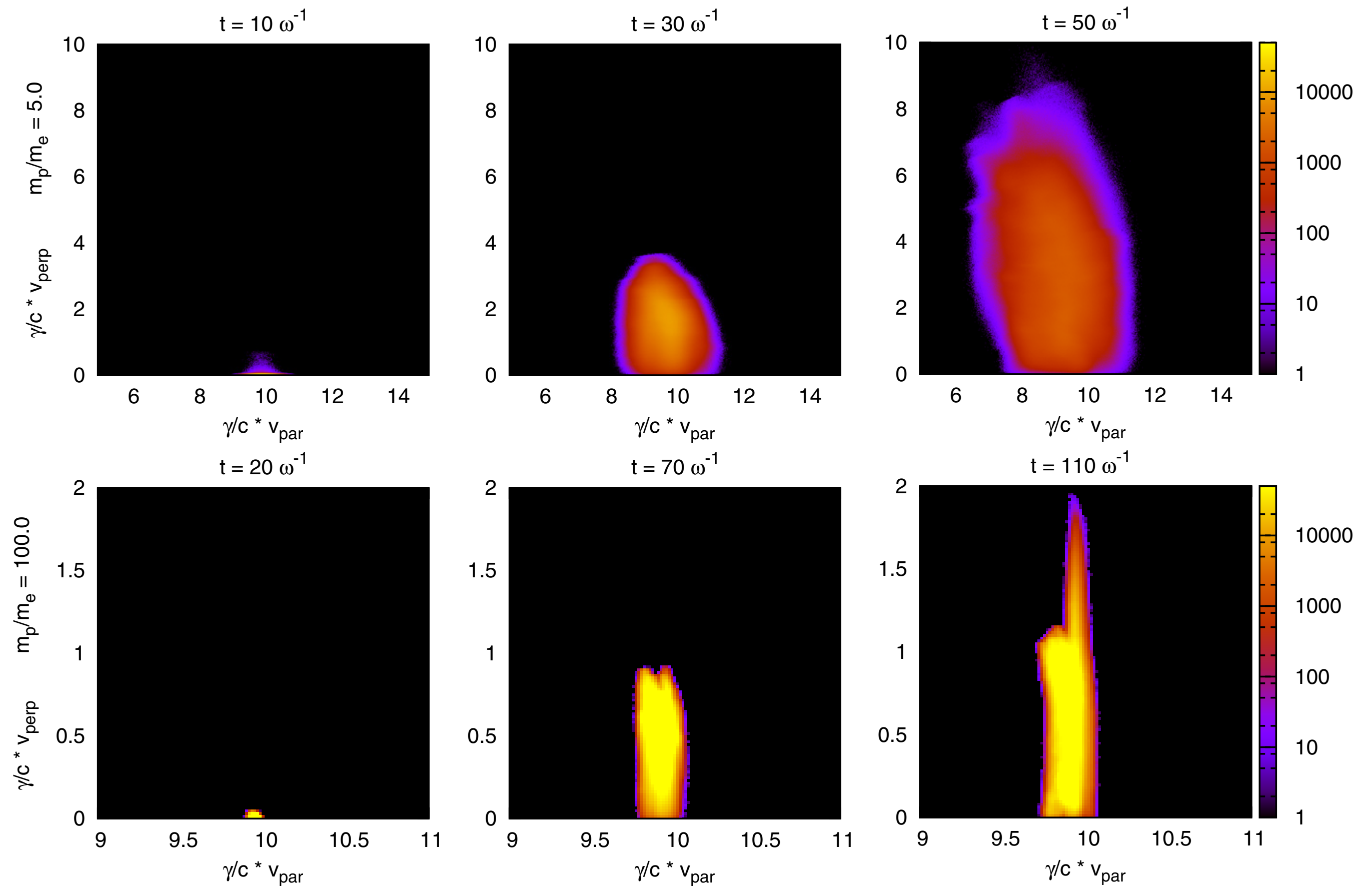

Figure 5. Development of the absolute value of the momentum distributions ($v_{\perp}/c \cdot \gamma$ over $v_{||}/c \cdot \gamma$) of all the protons parallel and perpendicular to the direction of the original flow in the lab rest frame. First, one can state that most of the particle acceleration happens in the transverse direction. Second, for a mass ratio of $m_p/m_e = 5.0$ the protons are getting accelerated over the entire time span, while for the higher mass ratio ($m_p/m_e = 100.0$) their acceleration starts at a later time during the simulation.

(A color version of this figure is available in the online journal.)

is stretched from $\gamma \approx 5$ to $\gamma \approx 15$. The particle energy is converted into perpendicular field energy which in turn accelerates the particles. We want to stress an interesting feature of the different particle distributions in the diverse simulations: both simulations have a proton distribution which is strongly elongated in the perpendicular direction and an electron distribution whose center is below the initial $\gamma = 10$ and extends more or less equal in the parallel and perpendicular directions. In the high mass case, it is obvious that the electrons are partially decelerated to lower energies.

In Figure 6, we show a one-dimensional plot of the temporal evolution of the total momentum distribution of all the particles (from both proton and pair-proton stream) in the lab frame. Particles moving in the negative (positive) z-direction are plotted with a negative (positive) total momentum and the narrow peak for each time shows the protons, the broad ones represent the electrons/positrons. One can see that most of the acceleration of the electrons and positrons is happening between $20\omega_p^{-1}$ and $70\omega_p^{-1}$, the protons still gain more energy until about $110\omega_p^{-1}$. This corresponds with the behavior of the particles seen in Figures 4 and 5.

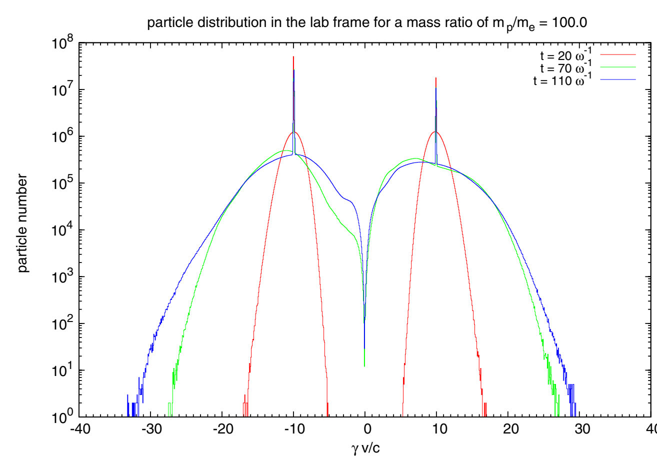

Figure 6. Time evolution of all particles' (both proton and pair-proton stream particles) momentum distribution in the lab frame for a mass ratio of $m_p/m_e = 100.0$. Particles moving to the left (proton stream) are shown with a negative total momentum, particles moving to the right (pair-proton stream) with a positive one. The narrow peak for each time shows the protons, the broad ones represent the electrons/positrons.

(A color version of this figure is available in the online journal.)

5. DISCUSSION AND SUMMARY

We have conducted several simulations of counterstreaming plasmas with different mass ratios $1.0 < m_p/m_e < 100.0$ in order to investigate the influence of the mass ratio on the development of two-stream instabilities. We can draw two major conclusions from our simulations: (1) the physics of acceleration in mixed counterstreaming plasmas can be understood by using

PiC simulations and (2) we are able to show that there is indeed a strong implication of the mass ratio on the results but in order to extrapolate the behavior to the physical mass ratio one still needs to perform some simulations with a higher mass ratio of 200 or 500.

We are able to demonstrate that the mass ratio has a qualitative and not only quantitative effect on the simulated physics. For very low mass ratios, only one instability develops which changes for mass ratios around 50. Taking these findings as a starting point we conclude that further simulations of counter-streaming plasma have to be conducted with mass ratios of 100 and above to find the correct physical behavior. A quantitative change has also been found: for mass ratios >20 the instability develops more slowly but also lasts longer (cf. Figure 1) because the flux tubes can be sustained for a greater time span. This can be explained by a two-stage instability that can be seen especially in the highest mass ratios. Here, in an initial phase a pair instability develops as in pair-only plasmas resulting in several flux tubes. In some of the flux tubes the (lighter) electrons and positrons are streaming and these are developing much stronger. After reaching its maximum the light-particle instability decreases and some other flux tubes (carrying mostly the heavier protons) grow stronger (see Figure 3).

Besides the investigation of the nature of the instability itself the acceleration of particles was a subject of research. From two-dimensional plots of particle momentum parallel versus perpendicular to the original streaming direction in the lab rest frame we concluded that most of the particle acceleration happens in the transverse direction. Furthermore, the two-stage process can also be observed here: while light and heavy particles are accelerated almost simultaneously for the low mass ratio simulations, the electrons are accelerated stronger and earlier compared to the protons in the high mass ratio simulations. Additionally, at a later stage the electron distribution stays almost the same while the much heavier protons still gain energy (see Figures 4 and 5). This gives important insight into the fundamental acceleration mechanism: only particles involved in the instability may be accelerated.

Since the instability itself and the restrictions on numerical parameters (i.e., the mass ratio) are now better understood, it is necessary to conceive the implications on the underlying physics of astrophysical jet phenomena. From this study it is not yet possible to impose strong limits on the possible composition of jets, since the major difference between pair and mixed plasma seems to be the time scale of how the instability develops. Obviously, an extensive parameter study is necessary to cover the full range of possible physics. Therefore, in a next stage the influence of the composition of the background and jet plasma on the particle acceleration shall be investigated.

T.B. thanks the Deutsches Zentrum für Luft- und Raumfahrt and the LISA-Germany Collaboration for funding. O.E. and U.G. are grateful for funding from the Elite Network of Bavaria and F.S. thanks the Deutsche Forschungsgemeinschaft (DFG SP 1124/1). Simulations have been conducted at Hochleistungsrechenzentrum Stuttgart under grant "iotmrofi."

REFERENCES

Boris, J. P. 1970, The Acceleration Calculation from a Scalar Potential, Plasma Physics Laboratory Report MATT-769
Buneman, O. 1958, Phys. Rev. Lett., 1, 8
Chang, P., Spitkovsky, A., & Arons, J. 2008, ApJ, 674, 378
Dieckmann, M. E., Shukla, P. K., & Drury, L. O. C. 2008, ApJ, 675, 586
Esirkepov, T. Z. 2001, Comput. Phys. Commun., 135, 144
Fermi, E. 1949, Phys. Rev., 75, 1169
Fonseca, R. A., Martins, S. F., Silva, L. O., Tonge, J. W., Tsung, F. S., & Mori, W. B. 2008, Plasma Phys. Control. Fusion, 50, 124034
Frederiksen, J. T., Hededal, C. B., Haugbølle, T., & Nordlund, Å. 2004, ApJ, 608, L13
Hededal, C. B., Haugbølle, T., Frederiksen, J. T., & Nordlund, Å. 2004, ApJ, 617, L107
Hededal, C. B., & Nishikawa, K.-I. 2005, ApJ, 623, L89
Hockney, R. W., & Eastwood, J. W. 1988, Computer Simulation Using Particles (Bristol: Hilger)
Martins, S. F., Fonseca, R. A., Silva, L. O., & Mori, W. B. 2009, ApJ, 695, L189
Nishikawa, K.-I., Hardee, P., Richardson, G., Preece, R., Sol, H., & Fishman, G. J. 2003, ApJ, 595, 555
Nishikawa, K.-I., Hardee, P., Richardson, G., Preece, R., Sol, H., & Fishman, G. J. 2005, ApJ, 622, 927
Nishikawa, K.-I., Hardee, P. E., Hededal, C. B., & Fishman, G. J. 2006, ApJ, 642, 1267
Nishikawa, K.-I., et al. 2008, in AIP Conf. Ser. 1085, New Relativistic Particle-In-Cell Simulation Studies of Prompt and Early Afterglows from GRBs, ed. F. A. Aharonian, W. Hofmann, & F. Rieger (New York: AIP), 589
Nishikawa, K., et al. 2010, IJMPD, 19, 715
Ramirez-Ruiz, E., Nishikawa, K.-I., & Hededal, C. B. 2007, ApJ, 671, 1877
Silva, L. O., Fonseca, R. A., Tonge, J. W., Dawson, J. M., Mori, W. B., & Medvedev, M. V. 2003, ApJ, 596, L121
Spitkovsky, A. 2008a, ApJ, 673, L39
Spitkovsky, A. 2008b, ApJ, 682, L5
Taflove, A., & Hagness, S. C. 2005, Computational Electrodynamics: The Finite-Difference Time-Domain Method (3rd ed.; Norwood, MA: Artech House)
Weibel, E. S. 1959, Phys. Rev. Lett., 2, 83
Yee, K. 1966, IEEE Trans. Antennas Propag., 14, 302